α-decay half-lives of superheavy nuclei within a one-parameter model*

Li-Qian Qi (齐立倩)[1,2,3] Hong-Min Wang (王宏民)[4] Jian-Po Cui (崔建坡)[1,2,3]
Yan-Zhao Wang (王艳召)[1,2,3,5,6†] Jian-Zhong Gu (顾建中)[6‡]

[1]Department of Mathematics and Physics, Shijiazhuang Tiedao University, Shijiazhuang 050043, China
[2]Institute of Applied Physics, Shijiazhuang Tiedao University, Shijiazhuang 050043, China
[3]Hebei Research Center of the Basic Discipline Engineering Mechanics, Shijiazhuang Tiedao University, Shijiazhuang 050043, China
[4]Physics Department, Army Academy of Armored Forces, PLA, Beijing 100072, China
[5]Hebei Key Laboratory of Physics and Energy Technology, North China Electric Power University, Baoding 071000, China
[6]China Institute of Atomic Energy, P. O. Box 275 (10), Beijing 102413, China

Abstract: The α-decay half-lives of superheavy nuclei (SHN) with charge numbers $Z \geq 104$ are investigated by employing a phenomenological one-parameter model based on quantum-mechanical tunneling through a potential barrier, where both the centrifugal and overlapping effects have been considered. It is shown that the experimental α-decay half-lives of the 81 SHN are reproduced well. Moreover, the order of magnitude for the α-particle preformation probability inside a parent nucleus (S_α) is found to be 10^{-2}. Then, within this model, the S_α values and α-decay half-lives of Z = 118−120 isotopes are predicted by inputting the α-decay energies (Q_α) extracted from the relativistic continuum Hartree-Bogoliubov (RCHB) theory, Duflo-Zuker 19 (DZ19, where 19 denotes the number of fitting parameters) model, improved Weizsacker-Skyrme (lMWS) model, and machine learning (ML) approach. By analyzing the evolutions of Q_α, S_α and α-decay half-lives of Z = 118−120 isotopes with the neutron number N of the parent nucleus, it is found that the shell effect at N = 184 is evident for all nuclear mass models. Meanwhile, for the case of the RCHB, N = 172 is determined as a submagic number. However, the submagic number at N = 172 is replaced by N = 178 for the ML approach.

Keywords: α-decay, superheavy nuclei, preformation probability, half-life

DOI: 10.1088/1674-1137/addcc8 **CSTR:** 32044.14.ChinesePhysicsC.49094102

I. INTRODUCTION

Studying the structure and properties of superheavy nuclei (SHN) has been a challenging and attractive subject for researchers [1−5]. In recent years, owing to the construction of a new generation of accelerators and the development of detection technology, the synthesis of elements with $Z \lesssim 118$ has been achieved through a hot fusion reaction with ^{48}Ca as a projectile or cold fusion using the double magic target ^{208}Pb or its neighbor ^{209}Bi as a target [6−19]. In synthesis, owing to the extremely low production cross-sections and short lifetimes of the SHN, it is difficult to detect and identify the new elements or isotopes directly. It is well known that α-decay is one of the main decay modes for SHN and it provides an efficient method for the identification of new superheavy elements or isotopes by detecting the α-decay chains from unknown nuclei to known nuclei with the help of the parent-daughter correlation [11, 20, 21]. Moreover, studying α-decay contributes to providing reliable information on the nuclear structure, including the ground-state lifetime, released energies, magic numbers, spin-parity, and nuclear interaction [7, 22−27]. Hence, the α-decay plays an indispensable role in theoretical and experimental studies of SHN.

α-decay was first explained in the 1920s by Gamow [28] and by Gurney and Condon [29] as a fundamental quantum tunneling effect, which is considered to be the first successful quantum description on nuclear phenomenon. Since then, based on this physical picture, numerous phenomenological and microscopic models, such as the effective liquid drop model [30−33], generalized liquid drop model [34, 35], cluster model [36−40], density-dependent M3Y effective interaction [41, 42], and uni-

Received 12 April 2025; Accepted 23 May 2025; Published online 24 May 2025

* Supported by the S&T Program of Hebei (236Z4601G); Scientific Research Foundation for the Introducing Returned Overseas Chinese Scholars of Hebei Province (C20230360); Foundation of Hebei Education Department (QN2021134); Key Laboratory of High Precision Nuclear Spectroscopy, Institute of Modern Physics, Chinese Academy of Sciences (IMPKFKT2021002); and Key Project of Natural Science Foundation for Basic Discipline Research of Hebei Province (A2023210064)

† E-mail: yanzhaowang09@126.com
‡ E-mail: gujianzhong2000@aliyun.com

fied fission model [43−45], have been developed to pursue a quantitative description of α-decay half-lives. In addition, a series of semi-empirical formulas, such as the Royer formula [46], universal decay law [47−51], and universal formula [52−54], have been proposed to calculate the α-decay half-lives. It has been found that these models and semi-empirical formulas can reproduce the experimental α-decay half-lives more or less satisfactorily [30−54].

The preformation probability S_α is an important physical quantity for α-decay half-life. However, it is difficult to obtain accurate S_α values of various nuclei. Thus, when estimating the α-decay half-lives, the empirical S_α values must be used [53, 55−58]. Moreover, these S_α values are strongly dependent on the models [59]. As a result, the order of magnitude of the calculated half-life is different when employing the S_α values extracted from different models. Therefore, it is very important and necessary to use a model that can calculate the S_α values reasonably to estimate the α-decay half-lives. Among the numerous α-decay models, the one-parameter model proposed by Tavares *et al.* is such a model that can estimate α-decay half-lives accurately because the S_α values can be extracted by a WKB-integral approximation [60]. Furthermore, the proton and cluster radioactivity were described successfully by this model [61−63]. In recent years, some new SHN have been synthesized and numerous experimental data on α-decay have been provided. These experimental data provide a basis for testing the one-parameter model. Therefore, it is necessary to extend this model to study the α-decay half-lives of SHN. This constitutes the first motivation of this article. Moreover, the synthesis of Z = 119 and 120 elements is the next aim for nuclear scientists [64−66], and therefore, the second motivation of the present study is to predict the α-decay half-lives of Z = 119 and 120 isotopes or their neighbors within this model. We hope that these predictions will be helpful for future experiments.

This remainder of this paper is organized as follows. In Sec. II, the theoretical framework is introduced. The results and discussions are presented in Sec. III. In the final section, several conclusions are provided.

II. THEORETICAL FRAMEWORK

In general, the half-life of α-decay is calculated by the following expression: $T_{1/2} = \lambda^{-1}\ln 2$, where $T_{1/2}$ is the half-life and λ is the decay constant. In the framework of the one-parameter model [60−63], λ is calculated by

$$\lambda = \lambda_0 S_\alpha P_{se}, \quad S_\alpha = \mathrm{e}^{-G_{ov}}, \quad P_{se} = \mathrm{e}^{-G_{se}}, \tag{1}$$

where λ_0 is the assault frequency on the barrier, G_{ov} represents the Gamow factor calculated in the overlapping barrier region in which the α-particle drives away from the parent nucleus until it reaches the contact configuration, G_{se} denotes the Gamow factor determined in the external separation region that spans from the aforementioned contact configuration to the separation point, and P_{se} is the corresponding penetration probability of the α-particle.

The quantity of λ_0 is usually estimated as

$$\lambda_0 = \frac{\upsilon}{2a} = \frac{2^{1/2}}{2a}\left(\frac{Q_\alpha}{\mu_0}\right)^{1/2}, \tag{2}$$

where υ is the relative velocity of the fragments and $a = R_p - R_a$ is the difference between the radius of the parent nucleus and the α-particle radius. μ_0 is the final reduced mass of the system. In this work, it is defined as $\mu_0 = \dfrac{A_d A_e}{A_d + A_e} m_p$. Here, A_d and A_e represent the mass numbers of the daughter nucleus and emitted particle, respectively. m_p denotes the nucleon mass.

In Eq. (1), G_{ov} and G_{se} are both calculated by the WKB-integral approximation and they can be expressed as

$$G_{ov} = \frac{2}{\hbar}\int_a^c \sqrt{2\mu_{ov}(r)[V_{ov}(r) - Q_\alpha]}\mathrm{d}r, \tag{3}$$

$$G_{se} = \frac{2}{\hbar}\int_c^b \sqrt{2\mu_{se}(r)[V_{se}(r) - Q_\alpha]}\mathrm{d}r, \tag{4}$$

where $\hbar$ is the reduced Planck constant, r is the center-of-mass distance between the emitted α-particle and daughter nucleus, $c = R_d + R_\alpha$ is the separation of fragments in the contact configuration, and b denotes the separation point where the total potential energy satisfies the condition $V(b) = Q_\alpha$. Here, R_α is the charge radius of the α-particle, whose value is 1.62 fm in this work. R_p and R_d are the radii of the parent and daughter nuclei, respectively, whose values are evaluated by the droplet model. The corresponding expressions are

$$R_i = \frac{Z_i}{A_i}R_{p'i} + \left(1 - \frac{Z_i}{A_i}\right)R_{n'i}, \quad i = p, d, \tag{5}$$

where $R_{p'i}$ and $R_{n'i}$ are given by

$$R_{ji} = r_{ji}\left[1 + \frac{5}{2}\left(\frac{w}{r_{ji}}\right)^2\right], \quad j = p', n'; \ i = p, d, \tag{6}$$

in which w = 1 fm denotes the diffuseness of the nuclear surface. r_{ji} represents the equivalent sharp radius of a proton ($j = p'$) or neutron ($j = n'$) density distribution of the parent nucleus ($i = p$) or daughter nucleus ($i = d$), respectively. According to the finite-range droplet model

theory of nuclei proposed by Möller *et al.*, the equivalent sharp radius can be extracted from the following expressions:

$$r_{p'i} = r_0(1+\overline{\epsilon_i})\left[1-\frac{2}{3}\left(1-\frac{Z_i}{A_i}\right)\left(1-\frac{2Z_i}{A_i}-\overline{\delta_i}\right)\right]A_i^{1/3}, \tag{7}$$

$$r_{n'i} = r_0(1+\overline{\epsilon_i})\left[1+\frac{2}{3}\frac{Z_i}{A_i}\left(1-\frac{2Z_i}{A_i}-\overline{\delta_i}\right)\right]A_i^{1/3}, \tag{8}$$

where $r_0 = 1.16$ fm, $i = p$ (parent) or d (daughter), and $\overline{\epsilon_i}$ and $\overline{\delta_i}$ can be expressed as

$$\overline{\epsilon_i} = \frac{1}{4e^{0.831A_i^{1/3}}} - \frac{0.191}{A_i^{1/3}} + \frac{0.0031Z_i^2}{A_i^{4/3}}, \tag{9}$$

$$\overline{\delta_i} = \left(1-\frac{2Z_i}{A_i}+0.004781\frac{Z_i}{A_i^{2/3}}\right)\Big/\left(1+\frac{2.52114}{A_i^{1/3}}\right). \tag{10}$$

In the overlapping barrier region ($a \le r \le c$, see Fig. 1), the reduced mass of the disintegration system $\mu_{ov}(r)$ and potential barrier $V_{ov}(r)$ appearing in Eq. (3) can be expressed as

$$\mu_{ov}(r) = \mu_0\left(\frac{r-a}{c-a}\right)^{\chi}, \quad \chi \geqslant 0, \tag{11}$$

$$V_{ov}(r) = Q_\alpha + (V_c - Q_\alpha)\left(\frac{r-a}{c-a}\right)^{q}, \quad q \geqslant 1, \tag{12}$$

with

$$V_c = \frac{2Z_de^2}{c} + \frac{l(l+1)\hbar^2}{2\mu_0c^2}, \tag{13}$$

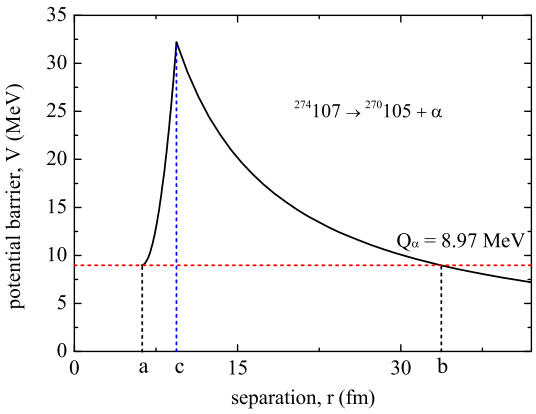

Fig. 1. (color online) Shape of the one-dimensional potential barrier for α-decay of $^{274}107$. The barrier from a to c is the overlapping region and that from c to b is the separation region.

in which $e^2 = 1.4399652$ MeV fm. l and Z_d represent the angular momentum carried by the α-particle and the charge number of the daughter nucleus, respectively. The mass power parameter χ in Eq. (11) and potential energy power parameter q in Eq. (12) are employed to characterize the variations in $\mu_{ov}(r)$ and $V_{ov}(r)$ in the overlapping region. According to Eqs. (3) and (11)−(13), the Gamow factor G_{ov} is analytically expressed as

$$G_{ov} = 0.4374702(c-a)g\left\{\mu_0\left[\frac{2Z_de^2}{c}+\frac{20.9008l(l+1)}{\mu_0c^2}-Q_\alpha\right]\right\}^{1/2}, \tag{14}$$

where

$$g = \left(1+\frac{\chi+q}{2}\right)^{-1}, \quad 0 < g \leqslant 2/3, \tag{15}$$

is the unique adjustable parameter of the model, the value of which is determined from a set of measured half-life values. According to Eqs. (11), (12), and (15), it can easily be observed that the parameter g is correlated to the reduced mass and interaction potential in the overlapping region.

In the separation region ($c \le r \le b$, see Fig. 1), the corresponding reduced mass of the disintegration system $\mu_{se}(r)$ becomes a constant. Meanwhile, the potential barrier $V_{se}(r)$ comprises superposition of the Coulomb and centrifugal potential barriers. As a result, $\mu_{se}(r)$ and $V_{se}(r)$ can be expressed as

$$\mu_{se}(r) = \mu_0, \tag{16}$$

$$V_{se}(r) = \frac{2Z_de^2}{r} + \frac{l(l+1)\hbar^2}{2\mu_0r^2}. \tag{17}$$

Combing Eqs. (4), (16), and (17), the Gamow factor G_{se} is written in a simple analytical form as follows:

$$G_{se} = 1.25988372Z_d\left(\frac{\mu_0}{Q_\alpha}\right)^{1/2}[F(x,y)+H(x,y)-f(x,y)], \tag{18}$$

with

$$F(x,y) = \frac{x^{1/2}}{2y}\times\ln\frac{[x(x+2y-1)]^{1/2}+x+y}{\frac{x}{y}\left[1+\left(1+\frac{x}{y^2}\right)^{1/2}\right]^{-1}+y}, \tag{19}$$

$$H(x,y) = \arccos\left\{\frac{1}{2}\left[1-\frac{1-\frac{1}{y}}{\left(1+\frac{x}{y^2}\right)^{1/2}}\right]\right\}^{1/2}, \tag{20}$$

$$f(x,y)=\left[\frac{1}{2y}\left(1+\frac{x}{2y}-\frac{1}{2y}\right)\right]^{1/2}, \tag{21}$$

where

$$x=\frac{20.9008l(l+1)}{\mu_0 c^2 Q_\alpha}, \quad y=\frac{Z_d e^2}{cQ_\alpha}. \tag{22}$$

Finally, the half-life of the α-decay is calculated by

$$T_{1/2}=1.0\times10^{-22}a\left(\frac{\mu_0}{Q_\alpha}\right)^{1/2}\mathrm{e}^{G_{ov}+G_{se}}. \tag{23}$$

III. RESULTS AND DISCUSSIONS

To proceed with a systematic analysis of the α-decay half-lives of SHN with $Z\geq104$, we first need to determine the g-value of Eq. (14), which has a certain influence on the strength of S_α as well as the half-lives. As the standard deviation (σ) represents the difference between the experimental and calculated half-lives, in this work, we follow the practice of Ref. [60] to determine the optimal g-value by minimizing σ within the following formula:

$$\sigma=\left[\frac{1}{n}\sum_{i=1}^{n}(\log_{10}T_{1/2}^{\mathrm{expt.}i}-\log_{10}T_{1/2}^{\mathrm{cal.}i})^2\right]^{1/2}, \tag{24}$$

where $\log_{10}T_{1/2}^{\mathrm{expt.}}$ and $\log_{10}T_{1/2}^{\mathrm{cal.}}$ are the decimal logarithms of the experimental and calculated half-lives, respectively. n is the number of α-decay events of SHN. By inputting the experimental Q_α values and half-lives obtained from Refs. [6−20, 68−71], the process for determining the optimal g-value is plotted in Fig. 2. It can be observed from Fig. 2 that the parameter g is determined to be 0.2038 when the minimum σ ($\sigma_{\min}$) is equal to 0.5127. Then, the half-lives of the 81 α-emitters are calculated within the one-parameter model by inputting the obtained optimal g-value. The detailed calculated results are listed in Table 1. In Table 1, column 1 represents the parent nuclei. Column 2 denotes the experimental Q_α values. The S_α values extracted using Eqs. (1), (14), and (15) are shown in column 3. Columns 4 and 5 are the decimal logarithms of the experimental half-lives and those of the calculated half-lives, respectively. Note that for α-decay of these SHN, the l values are selected as 0 because their spin-parities are not available. Therefore, the centrifugal potential contribution to the half-life is not considered. From Table 1, it can be observed that the S_α values are located between 6.12×10^{-2} and 7.15×10^{-2}, whose order of magnitude is consistent with those of the generalized liquid drop model [35, 72] and the study of Ismail *et al.* [73]. Next, to show the global deviation quantitatively, in addition to the abovementioned σ values, the average deviation $\overline{\sigma}$ is calculated using the following expression:

$$\overline{\sigma}=\frac{1}{n}\sum_{i=1}^{n}\left|\log_{10}T_{1/2}^{\mathrm{expt.}i}-\log_{10}T_{1/2}^{\mathrm{cal.}i}\right|. \tag{25}$$

Within Eq. (25), the obtained $\overline{\sigma}$ value of 81 SHN is 0.4377. This suggests that the experimental α-decay half-lives are reproduced effectively by this model.

To analyze the deviation of the experimental half-lives from the calculated ones further, the logarithm hindrance factor $\log_{10}HF$ is calculated by

$$\log_{10}HF=\log_{10}(T_{1/2}^{\mathrm{expt.}}/T_{1/2}^{\mathrm{cal.}}). \tag{26}$$

The $\log_{10}HF$ values within Eq. (26) are listed in the final column of Table 1 and the $\log_{10}HF$ values versus the neutron numbers N of the parent nuclei are plotted in Fig. 3. It is generally believed that if the $\log_{10}HF$ value is within a factor of 1.0, the calculated half-lives will be in agreement with the experimental data [5, 49, 50]. From the final column of Table 1 and Fig. 3, an agreement

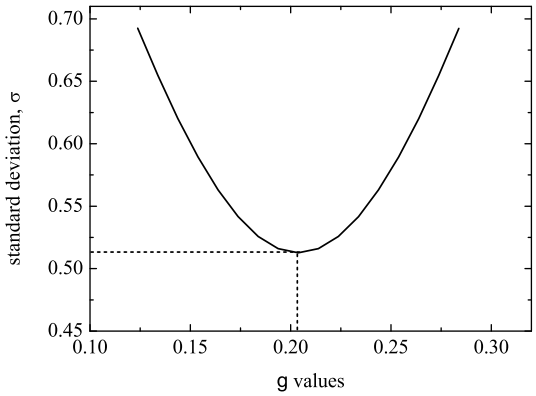

Fig. 2. Standard deviation σ as a function of the g-values.

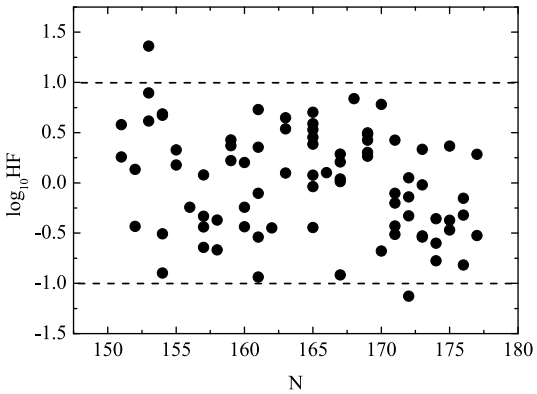

Fig. 3. The $\log_{10}HF$ values versus the neutron numbers N of parent nuclei for 81 SHN using the one-parameter model.

Table 1. Experimental and calculated α-decay half-lives of SHN with $Z \geqslant 104$.

Nuclei	Q_α /MeV	$S_\alpha(10^{-2})$	$\log_{10} T_{1/2}^{\text{expt.}}$ /s	$\log_{10} T_{1/2}^{\text{cal.}}$ /s	$\log_{10} HF$
$^{255}104$	9.05 [67]	6.63	0.65 [67]	0.39	0.26
$^{256}104$	8.93 [68]	6.59	0.32 [71]	0.75	−0.43
$^{258}104$	9.19 [68]	6.72	−0.97 [71]	−0.08	−0.90
$^{259}104$	9.13 [67]	6.70	0.41 [67]	0.09	0.33
$^{261}104$	8.65 [68]	6.53	0.91 [71]	1.55	−0.64
$^{263}104$	8.25 [67]	6.40	3.30 [67]	2.87	0.43
$^{256}105$	9.34 [68]	6.63	0.45 [71]	−0.13	0.58
$^{257}105$	9.21 [67]	6.59	0.39 [67]	0.25	0.14
$^{258}105$	9.50 [67]	6.72	0.75 [67]	−0.61	1.36
$^{259}105$	9.62 [68]	6.78	−0.29 [71]	−0.97	0.67
$^{270}105$	8.02 [6]	6.27	3.56 [6]	4.00	−0.44
$^{259}106$	9.80 [68]	6.73	−0.51 [71]	−1.12	0.62
$^{260}106$	9.90 [68]	6.78	−1.91 [71]	−1.40	−0.51
$^{261}106$	9.71 [68]	6.72	−0.73 [71]	−0.91	0.18
$^{263}106$	9.40 [68]	6.61	0.03 [71]	−0.05	0.08
$^{267}106$	8.32 [7]	6.25	2.80 [7]	3.34	−0.54
$^{269}106$	8.70 [68]	6.41	2.68 [71]	2.03	0.65
$^{271}106$	8.66 [8]	6.41	2.21 [8]	2.14	0.08
$^{260}107$	10.4 [67]	6.86	−1.46 [67]	−2.35	0.90
$^{261}107$	10.5 [67]	6.92	−1.93 [67]	−2.61	0.69
$^{265}107$	9.38 [9]	6.51	−0.03 [9]	0.34	−0.37
$^{266}107$	9.43 [10]	6.54	0.40 [10]	0.18	0.22
$^{267}107$	8.96 [10]	6.37	1.34 [10]	1.58	−0.24
$^{270}107$	9.06 [67]	6.44	1.78 [67]	1.24	0.54
$^{272}107$	9.14 [11]	6.49	0.91 [11]	0.95	−0.04
$^{274}107$	8.97 [6]	6.44	1.48 [6]	1.46	0.01
$^{264}108$	10.59 [67]	6.86	−2.80 [67]	−2.55	−0.24
$^{265}108$	10.47 [68]	6.82	−2.71 [71]	−2.27	−0.44
$^{266}108$	10.35 [67]	6.78	−2.64 [67]	−1.97	−0.67
$^{268}108$	9.62 [68]	6.52	0.15 [71]	−0.05	0.20
$^{269}108$	9.32 [12]	6.41	1.18 [12]	0.83	0.36
$^{270}108$	9.15 [20]	6.36	0.88 [20]	1.33	−0.45
$^{273}108$	9.73 [68]	6.61	−0.04 [71]	−0.43	0.39
$^{275}108$	9.44 [68]	6.52	−0.54 [71]	0.38	−0.92
$^{270}109$	10.18 [68]	6.64	−2.20 [71]	−1.26	−0.94
$^{274}109$	10.04 [13]	6.63	−0.35 [13]	−0.94	0.59
$^{275}109$	10.48 [14]	6.82	−2.01 [14]	−2.11	0.10
$^{276}109$	9.81 [67]	6.56	−0.14 [67]	−0.35	0.21
$^{278}109$	9.59 [6]	6.49	0.56 [6]	0.25	0.30
$^{267}110$	11.78 [68]	7.15	−5.00 [71]	−4.67	−0.33
$^{269}110$	11.51 [67]	7.06	−3.75 [67]	−4.12	0.37

Continued on next page

Table 1-continued from previous page

Nuclei	Q_α /MeV	$S_\alpha(10^{-2})$	$\log_{10}T^{\rm expt.}_{1/2}$ /s	$\log_{10}T^{\rm cal.}_{1/2}$ /s	$\log_{10}HF$
$^{270}110$	11.12 [68]	6.90	−3.69 [71]	−3.25	−0.44
$^{271}110$	10.87 [67]	6.81	−2.79 [67]	−2.68	−0.10
$^{273}110$	11.37 [67]	7.04	−3.77 [67]	−3.87	0.10
$^{275}110$	11.37 [70]	7.07	−3.37 [70]	−3.90	0.53
$^{277}110$	10.83 [67]	6.86	−2.39 [67]	−2.67	0.29
$^{279}110$	9.84 [8]	6.49	0.30 [8]	−0.13	0.43
$^{281}110$	8.86 [15]	6.14	2.35 [15]	2.86	−0.51
$^{272}111$	11.20 [67]	6.83	−2.42 [67]	−3.15	0.73
$^{278}111$	10.85 [67]	6.76	−2.38 [67]	−2.42	0.04
$^{279}111$	10.52 [67]	6.64	−0.77 [67]	−1.61	0.84
$^{280}111$	9.89 [11]	6.40	0.55 [11]	0.06	0.48
$^{281}111$	9.41 [16]	6.24	2.23 [16]	1.45	0.78
$^{282}111$	9.08 [6]	6.13	2.27 [6]	2.47	−0.20
$^{277}112$	11.62 [67]	6.94	−3.16 [67]	−3.86	0.70
$^{281}112$	10.46 [67]	6.52	−0.89 [67]	−1.15	0.27
$^{283}112$	9.67 [17]	6.24	0.58 [17]	1.01	−0.43
$^{284}112$	9.30 [18]	6.12	0.99 [18]	2.12	−1.13
$^{285}112$	9.32 [68]	6.13	1.51 [71]	2.04	−0.54
$^{278}113$	11.85 [67]	6.93	−3.62 [67]	−4.07	0.45
$^{282}113$	10.78 [67]	6.54	−1.15 [67]	−1.65	0.50
$^{283}113$	10.26 [14]	6.35	−0.99 [14]	−0.31	−0.68
$^{284}113$	10.11 [11]	6.30	−0.03 [11]	0.08	−0.10
$^{285}113$	9.84 [11]	6.22	0.51 [11]	0.84	−0.33
$^{286}113$	9.79 [67]	6.21	1.30 [67]	0.97	0.33
$^{285}114$	10.54 [19]	6.36	−0.33 [19]	−0.75	0.43
$^{286}114$	10.37 [68]	6.31	−0.46 [71]	−0.32	−0.14
$^{287}114$	10.16 [68]	6.24	−0.28 [71]	0.24	−0.53
$^{288}114$	10.07 [68]	6.22	−0.12 [71]	0.48	−0.60
$^{289}114$	9.97 [68]	6.19	0.38 [71]	0.75	−0.37
$^{287}115$	10.74 [68]	6.35	−0.92 [71]	−0.97	0.05
$^{288}115$	10.63 [68]	6.32	−0.72 [71]	−0.70	−0.02
$^{289}115$	10.49 [11]	6.28	−0.70 [11]	−0.34	−0.36
$^{290}115$	10.45 [6]	6.27	0.11 [6]	−0.25	0.37
$^{290}116$	10.99 [68]	6.36	−2.10 [71]	−1.32	−0.77
$^{291}116$	10.89 [68]	6.34	−1.55 [71]	−1.08	−0.47
$^{292}116$	10.77 [68]	6.30	−1.62 [71]	−0.80	−0.82
$^{293}116$	10.68 [68]	6.28	−1.10 [71]	−0.57	−0.52
$^{293}117$	11.18 [69]	6.36	−1.84 [69]	−1.51	−0.32
$^{294}117$	11.20 [6]	6.37	−1.29 [6]	−1.58	0.29
$^{294}118$	11.81 [68]	6.49	−2.85 [71]	−2.70	−0.15

between the calculated half-lives and experimental data is observed, except for the cases of ^{258}105 and ^{284}112. The agreement implies that the assumed S_α expression has a certain rationality. For some models, the inner potential barrier correlated to S_α is neglected. To compensate for this deficiency, the empirical or constant S_α is normally used [58, 74]. As a result, the accuracies and predicted powers of these models are not highly satisfactory. However, for the one-parameter model, the potential barrier is composed of the inner barrier in the overlapping region and external barrier in the separation region. The penetrability through the inner part of the potential is considered to represent S_α. Furthermore, the correlation between S_α and Q_α is considered, which can be seen from Eqs. (1) and (14). Thus, the S_α values can be extracted reasonably. In addition, relevant studies have suggested that the charge radius has an important influence on the α-decay half-life [39, 75, 76]. In the one-parameter model, the accurate radius expressions following the droplet model (Eqs. (5)−(10)) are included. Based on the two abovementioned reasons, most experimental α-decay half-lives are reproduced effectively. However, it is necessary to point out that there exist a set of expressions for the charge radius [77−81] except for the radius formulas of the droplet model. When other types of radius formulas are used to calculate the α-decay half-life within the one-parameter model, the calculated accuracy will change. However, if one wishes to improve the model accuracy, the parameters of the charge radius formulas need to be refitted using the experimental data of the α-decay.

Encouraged by the agreement between the calculated half-lives and experimental data, we attempted to predict the α-decay half-lives of Z = 118−120 isotopes within the one-parameter model. It is well known that the Q_α values play a crucial role in determining the half-lives. In recent years, various models for the nuclear masses have been developed to obtain the Q_α values [82−86]. In the present work, we selected the relativistic continuum Hartree-Bogoliubov (RCHB) [83], Duflo-Zuker 19 (DZ19) [84], improved Weizsacker-Skyrme model (IMWS) [85], and machine-learning (ML) [86] mass tables to obtain the Q_α values through the following relationship:

$$Q_\alpha = M - M_d - M_\alpha, \tag{27}$$

where M, M_d, and M_α represent the mass excesses of the parent nucleus, daughter nucleus, and emitted α-particle, respectively.

Then, the α-decay half-lives of the Z = 118−120 isotopes were calculated by inputting the Q_α values extracted from the abovementioned four types of nuclear mass tables. The Q_α values, corresponding S_α, and half-lives of the Z = 118−120 isotopes are listed in Table 2. From Table 2, it can be observed that (i) for a given nucleus, the Q_α values extracted from the four types of nuclear mass tables are different, which indicates that Q_α are strongly dependent on nuclear mass models; (ii) S_α is slightly dependent on the Q_α values; specifically, the larger the Q_α, the larger the S_α value, and vice versa; and (iii) the half-lives are sensitive to the Q_α values. For example, the Q_α value of ^{289}118 yielded by the RCHB theory is 2.82 MeV lower than that yielded by the DZ19 model, but the corresponding half-life difference is as high as approximately seven orders of magnitude. Hence, it is necessary to continue to develop a more accurate mass model by considering more physical ingredients.

Very recently, a newly synthesized nuclide ^{252}Rf was reported [87]. Its half-life is measured as 60^{+90}_{-30} ns, which is the shortest among all synthesized SHN. However, the research focused on its spontaneous fission and decay in high-K isomeric states and its α-decay half-life was not provided. Thus, we predicted its decimal logarithms of α-decay half-life within the one-parameter model by inputting the Q_α values extracted from the RCHB, DZ19, IMWS, and ML mass models, whose Q_α values are 10.71, 9.79, 9.66, and 9.87 MeV, respectively. The results for the decimal logarithms of the α-decay half-lives are –3.95, –1.68, –1.33, and –1.87 s, respectively. These values are much longer than its total half-life, which indicates that the dominant decay mode of ^{252}Rf is indeed the spontaneous fission. In addition, the Lawrence Berkeley National Laboratory announced that an SHN with Z = 116 was produced using titanium beams and two α-decay chains were observed from ^{290}Lv [88]. The Q_α values detected from the two α-decay chains were 10.32 and 10.98 MeV, respectively, which were close to the previous experimental data [68]. However, the precise α-decay half-lives were not measured. Within the one-parameter model by inputting the two new Q_α values, the decimal logarithms of α-decay half-lives were estimated as 0.44 and –1.30 s, respectively, which were greater than the half-life reported in Ref. [71]. Therefore, its α-decay half-life needs to be measured more accurately in future experiments.

Searching for the magic numbers of the SHN has been an interesting subject in modern nuclear physics. To obtain the magic numbers, the extracted Q_α values, corresponding S_α, and predicted $\log_{10}T_{1/2}$ values versus N are plotted in Fig. 4. Meanwhile, the locations of the magic numbers are marked by the dashed lines. It can be observed from Fig. 4 that, for the case of RCHB, the magic number effect at N = 172 and N = 184 is evident. This implies that the nuclei with N = 172 and N = 184 could be more stable and synthesized more easily than their neighborhoods. However, for the case of ML, the magic numbers are located at N = 178 and 184, respectively. Furthermore, the shell effect of N = 184 is stronger than that of N = 178. In addition, for the cases of DZ19 and IMWS, an apparent shell effect at N = 184 is observed. In fact, the shell effect at N = 184 is almost independent of

Table 2. Predicted $\log_{10}T_{1/2}$ values of $Z = 118-120$ isotopes by inputting the Q_α values extracted from the RCHB, DZ19, IMWS, and ML mass tables. The Q_α values and α-decay half-lives are measured in MeV and seconds, respectively. The symbol "–" indicates that the Q_α values are not available, and therefore, the corresponding $\log_{10}T_{1/2}$ values are not shown.

Nuclei	$Q_\alpha^{\rm RCHB}$ /MeV	$Q_\alpha^{\rm DZ19}$ /MeV	$Q_\alpha^{\rm IMWS}$ /MeV	$Q_\alpha^{\rm ML}$ /MeV	$S_\alpha^{\rm RCHB}$ (10^{-2})	$S_\alpha^{\rm DZ19}$ (10^{-2})	$S_\alpha^{\rm IMWS}$ (10^{-2})	$S_\alpha^{\rm ML}$ (10^{-2})	$\log_{10}T_{1/2}^{\rm RCHB}$ /s	$\log_{10}T_{1/2}^{\rm DZ19}$ /s	$\log_{10}T_{1/2}^{\rm IMWS}$ /s	$\log_{10}T_{1/2}^{\rm ML}$ /s
$^{289}118$	9.77	12.59	12.09	12.52	5.72	6.75	6.55	6.72	2.76	−4.31	−3.25	−4.17
$^{290}118$	9.50	12.38	12.18	12.46	5.65	6.67	6.60	6.71	3.60	−3.88	−3.47	−4.05
$^{291}118$	10.27	12.16	12.05	12.35	5.91	6.60	6.55	6.67	1.26	−3.43	−3.19	−3.84
$^{292}118$	10.97	11.95	12.07	12.10	6.16	6.53	6.57	6.59	−0.64	−2.99	−3.24	−3.32
$^{293}118$	10.94	11.75	11.92	12.17	6.16	6.46	6.53	6.62	−0.58	−2.54	−2.94	−3.48
$^{294}118$	10.92	11.56	11.89	12.06	6.16	6.40	6.52	6.59	−0.54	−2.12	−2.87	−3.25
$^{295}118$	10.88	11.36	11.78	11.83	6.16	6.33	6.49	6.51	−0.46	−1.67	−2.65	−2.77
$^{296}118$	10.78	11.18	11.89	11.61	6.13	6.28	6.55	6.44	−0.21	−1.25	−2.91	−2.27
$^{297}118$	10.65	11.00	11.83	12.03	6.09	6.22	6.53	6.61	0.12	−0.81	−2.80	−3.24
$^{298}118$	10.62	10.84	11.86	12.04	6.09	6.17	6.55	6.63	0.19	−0.40	−2.87	−3.27
$^{299}118$	10.50	10.67	11.76	11.98	6.06	6.12	6.53	6.61	0.50	0.02	−2.67	−3.14
$^{300}118$	10.48	10.52	11.75	11.81	6.06	6.08	6.53	6.56	0.54	0.42	−2.66	−2.80
$^{301}118$	10.27	10.37	11.68	11.95	6.00	6.03	6.51	6.62	1.11	0.83	−2.49	−3.11
$^{302}118$	10.62	10.23	11.65	11.90	6.13	5.99	6.51	6.61	0.13	1.20	−2.44	−3.01
$^{303}118$	12.21	11.18	12.40	12.53	6.74	6.34	6.82	6.88	−3.70	−1.33	−4.10	−4.38
$^{304}118$	12.66	11.92	12.36	12.98	6.94	6.64	6.82	7.08	−4.65	−3.09	−4.03	−5.29
$^{290}119$	9.98	12.95	12.74	13.07	5.71	6.79	6.70	6.84	2.46	−4.74	−4.34	−4.98
$^{291}119$	9.70	12.72	12.76	12.98	5.63	6.71	6.72	6.81	3.31	−4.32	−4.39	−4.82
$^{292}119$	10.57	12.50	12.75	12.90	5.92	6.63	6.73	6.79	0.74	−3.87	−4.38	−4.69
$^{293}119$	11.35	12.29	12.70	12.64	6.20	6.56	6.72	6.70	−1.29	−3.44	−4.29	−4.19
$^{294}119$	11.34	12.07	12.53	12.73	6.21	6.48	6.66	6.74	−1.28	−2.99	−3.96	−4.36
$^{295}119$	11.33	11.88	12.62	12.69	6.21	6.42	6.71	6.74	−1.27	−2.56	−4.16	−4.30
$^{296}119$	11.29	11.68	12.43	12.47	6.21	6.35	6.64	6.66	−1.18	−2.12	−3.79	−3.88
$^{297}119$	11.21	11.49	12.55	12.35	6.19	6.29	6.70	6.62	−1.00	−1.69	−4.05	−3.64
$^{298}119$	11.09	11.30	12.62	12.71	6.16	6.23	6.74	6.78	−0.71	−1.25	−4.20	−4.39
$^{299}119$	11.07	11.13	12.60	12.69	6.16	6.18	6.74	6.78	−0.68	−0.83	−4.17	−4.37
$^{300}119$	10.97	10.95	12.48	12.57	6.13	6.13	6.71	6.74	−0.43	−0.40	−3.95	−4.13
$^{301}119$	10.95	10.79	12.39	12.36	6.13	6.08	6.68	6.67	−0.40	0.01	−3.77	−3.69
$^{302}119$	10.70	10.63	12.32	12.43	6.06	6.03	6.66	6.70	0.25	0.43	−3.63	−3.86
$^{303}119$	11.17	10.48	12.23	12.35	6.23	5.99	6.64	6.68	−0.98	0.82	−3.46	−3.70
$^{304}119$	12.73	11.60	13.06	12.93	6.85	6.40	6.99	6.93	−4.50	−2.04	−5.15	−4.90
$^{305}119$	13.10	12.51	12.87	13.35	7.02	6.77	6.92	7.13	−5.24	−4.07	−4.80	−5.73
$^{291}120$	–	–	13.33	13.50	–	–	6.83	6.90	–	–	−5.21	−5.53
$^{292}120$	–	–	13.22	13.40	–	–	6.80	6.88	–	–	−5.03	−5.36
$^{293}120$	11.02	–	13.22	13.39	5.98	–	6.81	6.88	−0.14	–	−5.05	−5.36
$^{294}120$	11.91	12.63	13.23	13.17	6.31	6.59	6.83	6.80	−2.31	−3.89	−5.08	−4.96
$^{295}120$	11.88	12.42	13.17	13.26	6.31	6.51	6.81	6.85	−2.26	−3.44	−4.96	−5.14
$^{296}120$	11.88	12.21	13.16	13.27	6.32	6.45	6.82	6.87	−2.27	−3.02	−4.97	−5.18

Continued on next page

Table 2-continued from previous page

Nuclei	$Q_\alpha^{\rm RCHB}$ /MeV	$Q_\alpha^{\rm DZ19}$ /MeV	$Q_\alpha^{\rm IMWS}$ /MeV	$Q_\alpha^{\rm ML}$ /MeV	$S_\alpha^{\rm RCHB}$ (10^{-2})	$S_\alpha^{\rm DZ19}$ (10^{-2})	$S_\alpha^{\rm IMWS}$ (10^{-2})	$S_\alpha^{\rm ML}$ (10^{-2})	$\log_{10}T_{1/2}^{\rm RCHB}$ /s	$\log_{10}T_{1/2}^{\rm DZ19}$ /s	$\log_{10}T_{1/2}^{\rm IMWS}$ /s	$\log_{10}T_{1/2}^{\rm ML}$ /s
$^{297}120$	11.84	12.00	13.06	13.13	6.31	6.38	6.79	6.82	−2.19	−2.57	−4.78	−4.92
$^{298}120$	11.77	11.81	13.09	12.94	6.30	6.31	6.81	6.75	−2.05	−2.14	−4.86	−4.56
$^{299}120$	11.66	11.61	13.10	13.25	6.27	6.25	6.83	6.89	−1.80	−1.69	−4.89	−5.17
$^{300}120$	11.63	11.43	13.05	13.25	6.27	6.19	6.82	6.90	−1.75	−1.27	−4.81	−5.19
$^{301}120$	11.55	11.24	12.90	13.05	6.25	6.14	6.77	6.83	−1.57	−0.83	−4.53	−4.82
$^{302}120$	11.52	11.08	12.81	12.82	6.25	6.09	6.74	6.75	−1.51	−0.42	−4.37	−4.38
$^{303}120$	11.33	10.90	12.74	12.80	6.19	6.04	6.73	6.75	−1.06	0.01	−4.23	−4.35
$^{304}120$	11.73	10.75	12.66	12.69	6.34	5.99	6.70	6.72	−2.04	0.42	−4.08	−4.15
$^{305}120$	13.25	12.03	13.45	13.27	6.96	6.47	7.04	6.96	−5.25	−2.76	−5.64	−5.29
$^{306}120$	13.59	13.12	13.29	13.72	7.11	6.91	6.99	7.17	−5.90	−5.02	−5.35	−6.14

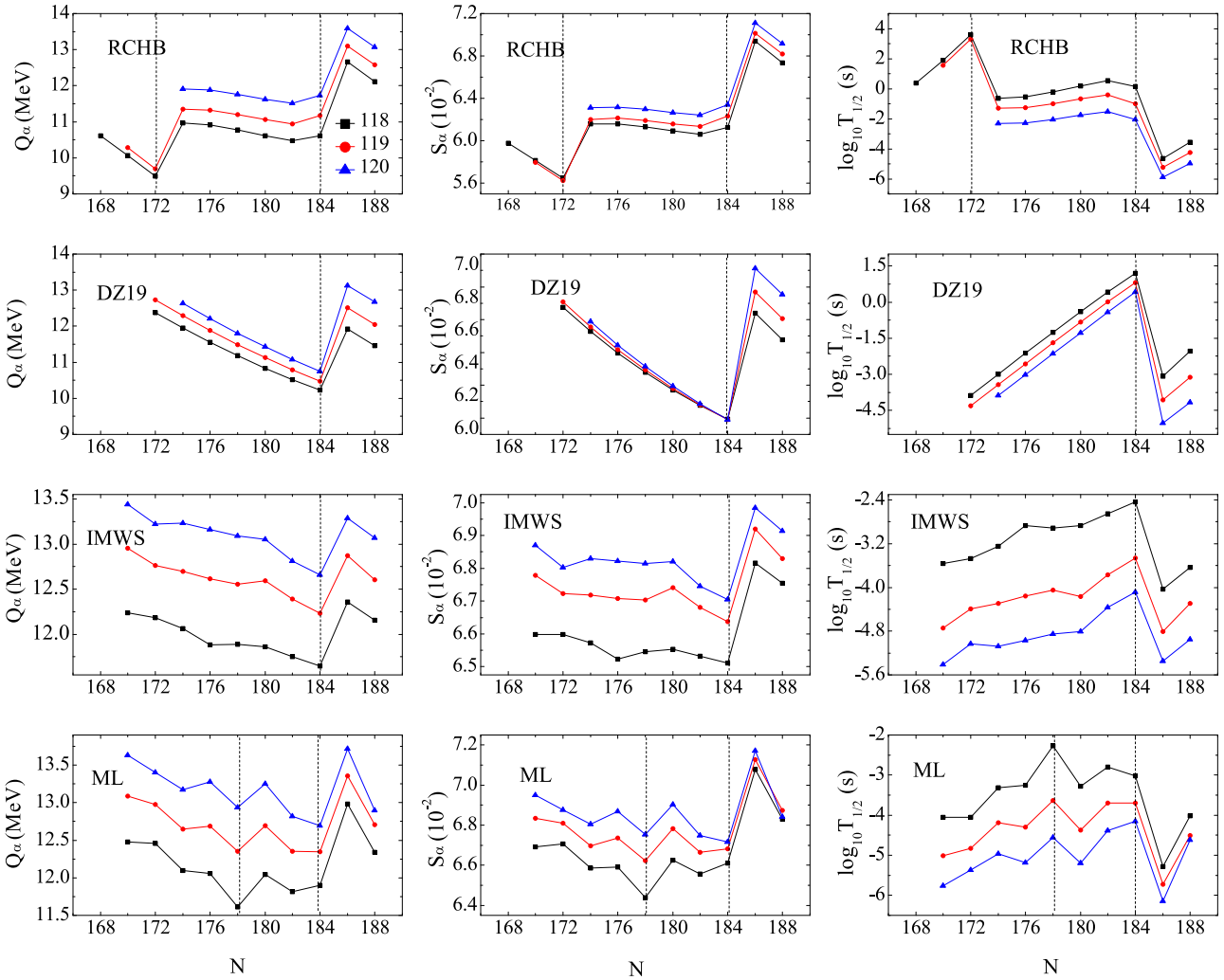

Fig. 4. (color online) Left panel: Extracted Q_α values of Z = 118−120 isotopes versus N for RCHB theory, DZ19, IMWS, and ML models. Middle panel: As in the left panel, but for the corresponding S_α values. Right panel: As in the left and middle panels, but for the corresponding $\log_{10}T_{1/2}$ values.

the models [93, 89]. However, the shell effects at $N = 172$ and 178 are strongly dependent on the models. Nonetheless, the shell effects of the SHN need to be verified by further experiments in the future.

V. CONCLUSIONS

In this study, the α-decay half-lives of SHN with $Z \geq 104$ were calculated using the one-parameter model. The comparison of the calculations and experimental data showed that the calculated half-lives were in good agreement with the experimental data. Moreover, the S_α values and α-decay half-lives of the $Z = 118$−120 isotopes were estimated by inputting the Q_α values extracted from the RCHB, DZ19, IMWS, and ML nuclear mass tables. It was shown that the order of magnitude of S_α was 10^{-2}. By analyzing the Q_α values, the corresponding S_α, and $\log_{10} T_{1/2}$ values versus the neutron number N, it was found that the shell effect at $N = 184$ was evident for all cases. Meanwhile, it was found that $N = 172$ was the submagic number for the RCHB theory. However, the submagic number at $N = 172$ was replaced by $N = 178$ for the ML approach. We hope that our study will be helpful for the synthesis of new SHN in the future. Finally, it is necessary to note that the two-proton radioactivity, especially its spectroscopic factor, has attracted attention in recent years [90−93]. However, it is challenging to obtain an accurate spectroscopic factor because the correlation between the two emitted protons is complex [90−95]. Therefore, it will be interesting to extend or improve the one-parameter model to extract the spectroscopic factor of the two-proton radioactivity, which is a work in progress.

References

[1] T. Wan, S. L. Tang, and Y. B. Qian, Chin. Phys. C **48**, 034103 (2024)
[2] G. Saxena, P. K. Sharma, and P. Saxena, Eur. Phys. J. A **60**, 50 (2024)
[3] Y. L. Zhang and Y. Z. Wang, Phys. Rev. C **97**, 014318 (2018)
[4] Y. Z. Wang, S. J. Wang, Z. Y. Hou *et al.*, Phys. Rev. C **92**, 064301 (2015)
[5] J. P. Cui, Y. L. Zhang, S. Zhang *et al.*, Phys. Rev. C **97**, 014316 (2018)
[6] J. Khuyagbaatar, A. Yakushev, Ch. E. Düllmann *et al.*, Phys. Rev. Lett. **112**, 172501 (2014)
[7] J. Dvorak, W. Brüchle, M. Chelnokov *et al.*, Phys. Rev. Lett. **100**, 132503 (2008)
[8] Yu. Ts. Oganessian, V. K. Utyonkov, Yu. V. Lobanov *et al.*, Phys. Rev. C **74**, 044602 (2006)
[9] Z. G. Gan, J. S. Guo, X. L. Wu *et al.*, Eur. Phys. J. A **20**, 385 (2004)
[10] P. A. Wilk, K. E. Gregorich, A. Türler *et al.*, Phys. Rev. Lett. **85**, 2697 (2000)
[11] Yu. Ts. Oganessian, F. Sh. Abdullin, S. N. Dmitriev *et al.*, Phys. Rev. Lett. **108**, 022502 (2012)
[12] S. Hofmann and G. Münzenberg, Rev. Mod. Phys. **72**, 733 (2000)
[13] Yu. Ts. Oganessian, V. K. Utyonkov, Yu. V. Lobanov *et al.*, Phys. Rev. C **76**, 011601(R) (2007)
[14] Yu. Ts. Oganessian, V. K. Utyonkoy, Yu. V. Lobanov *et al.*, Phys. Rev. C **69**, 021601(R) (2004)
[15] Ch. E. Düllmann, M. Schädel, A. Yakushev *et al.*, Phys. Rev. Lett. **104**, 252701 (2010)
[16] Yu. Ts. Oganessian, F. Sh. Abdullin, C. Alexander *et al.*, Phys. Rev. C **87**, 054621 (2013)
[17] Yu. Oganessian, J. Phys. G: Nucl. Part. Phys. **34**, R165 (2007)
[18] Yu. Ts. Oganessian, V. K. Utyonkov, Yu. V. Lobanov *et al.*, Phys. Rev. C **62**, 041604 (2000)
[19] P. A. Ellison, K. E. Gregorich, J. S. Berryman *et al.*, Phys. Rev. Lett. **105**, 182701 (2010)
[20] Yu. Ts. Oganessian, Radiochim. Acta **99**, 429 (2011)
[21] J. H. Hamilton, S. Hofmann, and Y. T. Oganessian, Ann. Rev. Nucl. Part. Sci. **63**, 383 (2013)
[22] J. G. Deng and H. F. Zhang, Phys. Rev. C **102**, 044314 (2020)
[23] E. Olsen and W. Nazarewicz, Phys. Rev. C **99**, 014317 (2019)
[24] D. T. Akrawy and A. H. Ahmed, Phys. Rev. C **100**, 044618 (2019)
[25] T. N. Ginter, K. E. Gregorich, W. Loveland *et al.*, Phys. Rev. C **67**, 064609 (2003)
[26] X. Y. Zhu, S. Luo, W. Gao *et al.*, Chin. Phys. C **48**, 074102 (2024)
[27] X. Liu, J. D. Jiang, X. J. Wu *et al.*, Chin. Phys. C **48**, 054101 (2024)
[28] G. Gamow and Z. Phys. **51**, 204 (1928).
[29] E. U. Condon and R. W. Gurney, Nature **122**, 439 (1928)
[30] M. G. Goncalves and S. B. Duarte, Phys. Rev. C **48**, 2409 (1993)
[31] S. B. Duarte and M. G. Goncalves, Phys. Rev. C **53**, 2309 (1996)
[32] F. Guzman, M. Goncalves and O. A. P. Tavares *et al.*, Phys. Rev. C **59**, R2339 (1999)
[33] J. P. Cui, F. Z. Xing, Y. H. Gao *et al.*, Commun. Theor. Phys. **76**, 035301 (2024)
[34] G. Royer, R. K. Gupta and V. Y. Denisov, Nucl. Phys. A **632**, 275 (1998)
[35] H. F. Zhang and G. Royer, Phys. Rev. C **77**, 054318 (2008)
[36] B. Buck, Phys. Rev. Lett. **72**, 1326 (1994)
[37] B. Buck, A. C. Merchant and S. M. Perez, Phys. Rev. C **45**, 2247 (1992)
[38] C. Xu and Z. Z. Ren, Phys. Rev. C **69**, 024614 (2004)
[39] Y. Z. Wang, F. Z. Xing, Y. Xiao *et al.*, Chin. Phys. C **45**, 044111 (2021)
[40] C. Xu and Z. Z. Ren, Phys. Rev. C **74**, 037302 (2006)
[41] P. R. Chowdhury, C. Samanta, and D. N. Basu, Phys. Rev. C **73**, 014612 (2006)
[42] C. Samanta, P. R. Chowdhury, and D. N. Basu, Nucl. Phys. A **789**, 142 (2007)
[43] T. B. Zhu, B. T. Hu, H. F. Zhang *et al.*, Commun. Theor. Phys. **55**, 307 (2011)
[44] J. M. Dong, H. F. Zhang, J. Q. Li *et al.*, Eur. Phys. J. A **41**,

197 (2009)
[45] K. P. Santhosh, R. K. Biju, and A. Joseph, J. Phys. G: Nucl. Part. Phys. **35**, 085102 (2008)
[46] G. Royer, J. Phys. G: Nucl. Part. Phys. **26**, 1149 (2000)
[47] C. Qi, F. R. Xu, R. J. Liotta *et al*., Phys. Rev. Lett. **103**, 072501 (2009)
[48] C. Qi, F. R. Xu, R. J. Liotta *et al*., Phys. Rev. C **80**, 044326 (2009)
[49] F. Z. Xing, H. Qi, J. P. Cui *et al*., Nucl. Phys. A **1028**, 122528 (2022)
[50] L. Q. Qi, J. P. Cui, Y. H. Gao *et al*., Nucl. Phys. A **1050**, 122929 (2024)
[51] F. Z. Xing, J. P. Cui, Y. H. Gao *et al*., Nucl. Phys. Rev. **40**, 511 (2023)(in Chinese)
[52] D. N. Poenaru, Phys. Rev. C **65**, 054308 (2002)
[53] D. N. Poenaru, R. A. Gherghescu, and W. Greiner, Phys. Rev. C **83**, 014601 (2011)
[54] D. N. Poenaru and R. A. Gherghescu, Phys. Rev. C **97**, 044621 (2018)
[55] H. F. Zhang, G. Royer, Y. J. Wang *et al*., Phys. Rev. C **80**, 057301 (2009)
[56] D. D. Ni and Z. Z. Ren, Nucl. Phys. A **828**, 348 (2009)
[57] Y. B. Qian and Z. Z. Ren, Nucl. Phys. A **852**, 82 (2011)
[58] O. Nagib, Phys. Rev. C **101**, 014610 (2020)
[59] S. M. S. Ahmed, R. Yahaya, S. Radiman *et al*., Eur. Phys. J. A **51**, 13 (2015)
[60] O. A. P. Tavares, E. L. Medeiros, and M. L. Terranova, J. Phys. G: Nucl. Part. Phys. **31**, 129 (2005)
[61] E. L. Medeiros, M. M. N. Rodrigues, S. B. Duarte, and O. A. P. Tavares, J. Phys. G: Nucl. Part. Phys. **32**, B23 (2006)
[62] O. A. P. Tavares and E. L. Medeiros, Phys. Scr. **86**, 015201 (2012)
[63] E. L. Medeiros, M. M. N. Rodrigues, S. B. Duarte *et al*., Eur. Phys. J. A **34**, 417 (2007)
[64] C. E. Düllmann, EPJ Web Conf. **163**, 00015 (2017)
[65] S. Hofmann, S. Heinz, R. Mann *et al*., Eur. Phys. J. A **52**, 1 (2016)
[66] Yu. Ts. Oganessian, V. K. Utyonkov, N. D. Kovrizhnykh *et al*., Phys. Rev. C **106**, L031301 (2022)
[67] NuDat2.7, http://www.nndc.bnl.gov.
[68] M. Wang, G. Audi, F. G. Kondev *et al*., Chin. Phys. C **41**, 030003 (2017)
[69] Yu. Ts. Oganessian, F. Sh. Abdullin, P. D. Bailey *et al*., Phys. Rev. Lett. **104**, 142502 (2010)
[70] Yu. Ts. Oganessian, V. K. Utyonkov, M. V. Shumeiko *et al*., Phys. Rev. C **109**, 054307 (2024)
[71] G. Audi, F. G. Kondev, M. Wang *et al*., Chin. Phys. C **41**, 030001 (2017)
[72] J. G. Deng and H. F. Zhang, Chin. Phys. C **45**, 024104 (2021)
[73] M. Ismail, A. Y. Ellithi, A. El-Depsy *et al*., Int. J. Mod. Phys. E **26**, 1750026 (2017)
[74] F. Z. Xing, J. P. Cui, Y. Z. Wang *et al*., Chin. Phys. C **45**, 124105 (2021)
[75] Y. B. Qian, Z. Z. Ren, and D. D. Ni, Rhys. Rev. C **87**, 054323 (2013)
[76] Y. B. Qian and Z. Z. Ren, Nucl. Phys. A **945**, 134 (2016)
[77] Y. Y. Cao and J. Y. Guo, Acta Phys. Sin. **69**, 162101 (2020)
[78] Z. Q. Sheng, G. W. Fan, J. F. Qian *et al*., Eur. Phys. J. A **51**, 40 (2015)
[79] S. Q. Zhang, J. Meng, S. G. Zhou *et al*., Eur. Phys. J. A **13**, 285 (2002)
[80] N. Wang and T. Li, Rhys. Rev. C **88**, 011301(R) (2013)
[81] L. Tang, Z. H. Zhang, Nucl. Phys. Rev. **41**, 927 (2024) (in Chinese)
[82] H. M. Wu, H. Jiang, and C. W. Dai, Nucl. Phys. Rev. **42**, 25 (2025) (in Chinese)
[83] X. W. Xia, Y. Lim, P. W. Zhao *et al*., Atom. Data Nucl. Data **121**, 1 (2018)
[84] C. Qi, J. Phys. G: Nucl. Part. Phys. **42**, 045104 (2015)
[85] N. N. Ma, H. F. Zhang, X. J. Bao *et al*., Chin. Phys. C **43**, 044105 (2019)
[86] Z. P. Gao, Y. J. Wang, H. L. Lü *et al*., Nucl. Sci. Tech. **32**, 109 (2021)
[87] J. Khuyagbaatar, P. Mosat, J. Ballof *et al*., Phys. Rev. Lett. **134**, 022501 (2025)
[88] J. M. Gates, R. Orford, D. Rudolph *et al*., Phys. Rev. Lett. **133**, 172502 (2024)
[89] N. Wang, M. Liu, X. Z. Wu *et al*., Phys. Lett. B **734**, 215 (2014)
[90] Y. Z. Wang, F. Z. Xing, J. P. Cui *et al*., Chin. Phys. C **47**, 084101 (2023)
[91] Y. Z. Wang, F. Z. Xing, W. H. Zhang *et al*., Phys. Rev. C **110**, 064305 (2024)
[92] L. Zhou, S. M. Wang, D. Q. Fang *et al*., Nucl. Sci. Tech. **33**, 105 (2022)
[93] M. Pfützner, M. Karny, L. V. Grigorenko *et al*., Rev. Mod. Phys. **84**, 567 (2012)
[94] J. P. Cui, Y. H. Gao, Y. Z. Wang *et al*., Rhys. Rev. C **101**, 014301 (2020)
[95] J. D. Jiang, X. Liu, D. M. Zhang *et al*., Chin. Phys. C **48**, 104108 (2024)